Multilayer Coatings for High-Energy Optics for Astrophysics

Silicon mirrors for the XEUS X-ray telescope pore optics: microroughness characterization

*Issued by **D. Spiga** (INAF/OAB, Merate, Italy)*

*Measurements performed by **D. Spiga**, **G. Sironi**, **V. Cotroneo**, **R. Canestrari** (INAF/OAB) and **G. Destefanis** (Media-Lario techn., Bosisio Parini, Italy)*

*Multilayer coatings deposited by **V. Mattarello** (Media-Lario Techn.) at INFN/Laboratori Nazionali di Legnaro (Padova, Italy)*

Contents

Applicable Documents

[AD1] M. Bavdaz, et al., *Status of X-ray optics Development for the XEUS Mission*, **SPIE Proc**., 5488, 829 (2004)

[AD2] *ESA silicon substrate microroughness characterization*, INAF/OAB Internal Report 01/05

[AD3] Media Lario Document MX-PL-ML-001 *Alternative Coatings for Nickel Mirrors - Test Plan*

Reference Documents

[RD1] ISO 10110 Standard: *Optics and Optical Instruments-Preparation of Drawings for Optical Elements and Systems: A User's guide*. Washington DC: Optical Society of America

[RD2] E. L Church, et al., *Relationship between surface scattering and microtopographic features*. **Optical Engineering**, vol.18, p. 125-136 (1979)

[RD3] D. Spiga et al., *Multilayer coatings for X-ray mirrors: extraction of stack parameters from X-ray reflectivity scans and comparison with Transmission Electron Microscope results*. **Optical Engineering**, Vol. 46, No. 8, pp. 086501

[RD4] D. Spiga, *Analytical evaluation of the X-ray scattering contribution to imaging degradation in grazing-incidence X-ray telescopes*, **Astronomy and Astrophysics**, Vol. 468, issue 2, pp. 775-784

Acronyms

AFM Atomic Force Microscope
ESA European Space Agency
HEW Half-Energy Width
INAF Istituto Nazionale di AstroFisica / *Italian Institute for Astrophysics*
INFN Istituto Nazionale di Fisica Nucleare */National Institute for Nuclear Physics*
LNL Laboratori Nazionali di Legnaro */National Laboratories in Legnaro*
LTP Long Trace Profilometer
MLT Media-Lario Technologies
OAB Osservatorio Astronomico di Brera / *Brera Astronomical Observatory*
PPM Pythonic Program for Multilayers
PSD Power Spectral Density
XRR X-Ray Reflectivity
XRS X-Ray Scattering

1. Aim of the document

Aim of this document is to present roughness characterizations of 6 uncoated Silicon strips (size: 100 mm x 10 mm x 1 mm) provided by ESA and the X-ray and surface characterization of Mo/Si samples deposited onto substrates of the same kind. It is also of the same kind of substrates used to produce, after a chemical etching of one side of each stripe and an opportune assembly procedure, light-weight pore optics which is the present baseline for the realization of the XEUS telescope [AD1]. The present activity is the follow-up of a similar study performed in 2004 onto a Silicon sample, provided by ESA as well [AD2]. In this case, some Silicon samples have also been coated with multilayer films, deposited at INFN-LNL.

The strips characterization has been performed at INAF-OAB, also making use of some instrumentation available at *Media-Lario techn.*. We report here the results obtained in the multi-instrumental topographic analysis, by means of the following instrumentation:

- ✓ LTP Long Trace Profilometer
- ✓ WYKO Optical Profilometer
- ✓ PROMAP surface roughness imager
- ✓ AFM
- ✓ BEDE 1D X-ray triple axis Diffractometer

Most characterizations have been performed on the samples, *before and after the deposition of multilayer coating*, at INAF/OAB expressing the results in terms of Power-Spectral Density (PSD, [RD1]), i.e. along with the power spectrum of rough profiles, as traced at several locations of the samples in order to increase the statistical significance of the characterization. This representation of results enables a useful comparison of results retrieved from instruments having a specific spectral range of sensitivity, as the resulting PSDs should be consistent with each other in the common spectral ranges. In addition, the comparison of samples in terms of PSD also highlights the roughness modification (worsening of improvement) consequent to the multilayer coatings deposition. Finally, the PSD is the physical quantity that mainly determines the X-ray scattering (XRS), which is in turn responsible for the increasing degradation of imaging quality in X-ray optical systems for increasing photon energy [RD2].

Topographical characterizations reported in the following are based on digital maps/ profiles of representative regions of the Silicon samples: X-ray reflectivity tests permit an independent evaluation of the roughness, averaged over a larger fraction of the Silicon samples. In addition, LTP measurements also allowed us tracing the figure of the substrates. In the "Test Plan" document ([AD3]) a detailed description of the kind of instrumentations and measurements mentioned above, in addition to the typical performed analysis, are reported.

2. Uncoated Silicon strips: roughness characterization

The uncoated samples consist of 6 strips (10 cm long, 1 cm wide, 0.8 mm thick) 3 labelled by ESA as "Jan 06", and 3 as "Nov 05". We shall heretofore denote the samples of the first group with J1, J2, J3, whilst those of the second type with N4, N5, N6. The results will be separately provided for the two groups, even though the PSD will be given as averaged within each group of samples. The two sides of the samples are *conventionally* labelled with "A" and "B".

2.1 LTP profiles – planarity and roughness

The deviation of the Silicon strips from planarity have been measured by means of the optical LTP operated at INAF/OAB. Both sizes of the six strips were measured. During the profile scans acquisition, the samples were laid on an optical paper sheet. The surface profiles of the samples are in Fig. 1: for all samples but two (J1 and J3), the profiles on the two sides are not symmetric. This could indicate a non uniformity of the samples (a few micron) or a weight-induced deformation of samples at measurement time.

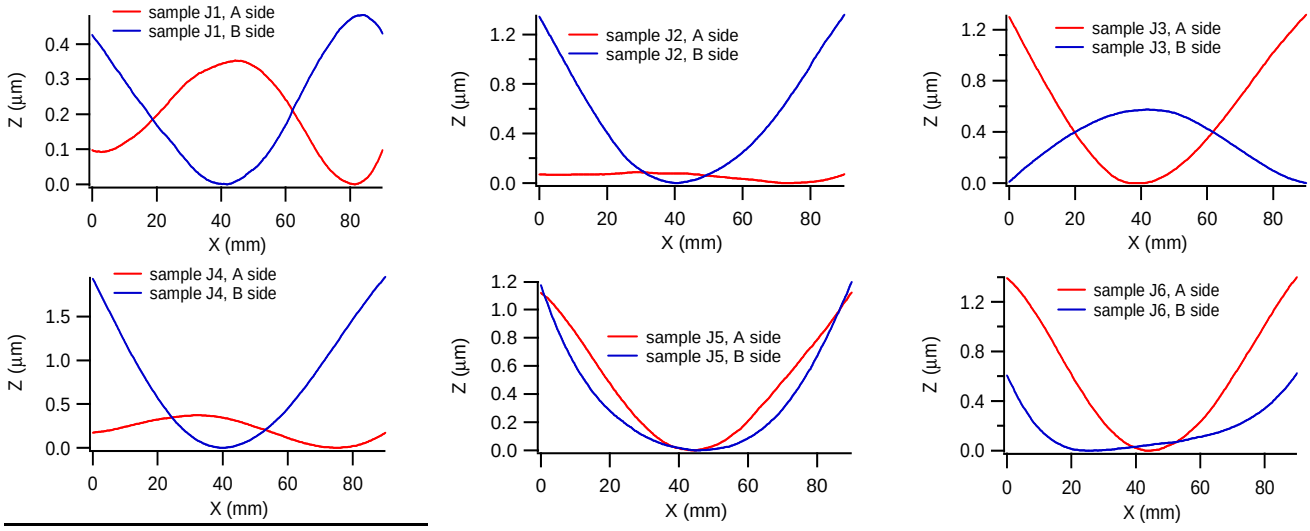

Fig. 1: LTP profiles of the Silicon strips.

The samples figure, as measured with LTP, highlights an improvement with respect to the case of sample characterized in [RD2]. In that case the peak-valley of the profile was 5.4 µm whilst in the present dataset the P-V does not exceed 2 µm. We list in Tab.1 the listed the P-V values that can be also derived from Fig.1.

In addition, we performed the subtraction of a 4^{th}-order polynomial from the profiles in Fig. 1, deriving thereby the noisy residuals that represent the low-frequency roughness of the samples. The PSD of residuals have been computed and averaged for the two groups of samples: the resulting PSD, as a function of the spatial wavelength, are shown in Fig. 2. The two PSDs are quite similar and fit a typical power-law spectrum: $P(f) = K_n/f^n$ where f is the spatial frequency.

The measured PSD is significant because it is well beyond the instrumental noise of the LTP in the frequency range $10^4 \div 600$ µm. The larger uncertainty is found at very low frequencies (1/f > 5 mm) as a probable consequence of residual environmental vibrations with a spectrum which also approximates a power-law.

Tab. 1: figure profiles P-V for the samples under test

Sample n.	**Side A**	**Side B**
J1	0.352 µm	0.483 µm
J2	0.085 µm	1.359 µm
J3	1.316 µm	0.575 µm
N4	0.374 µm	1.952 µm
N5	1.124 µm	1.197 µm
N6	1.397 µm	0.622 µm

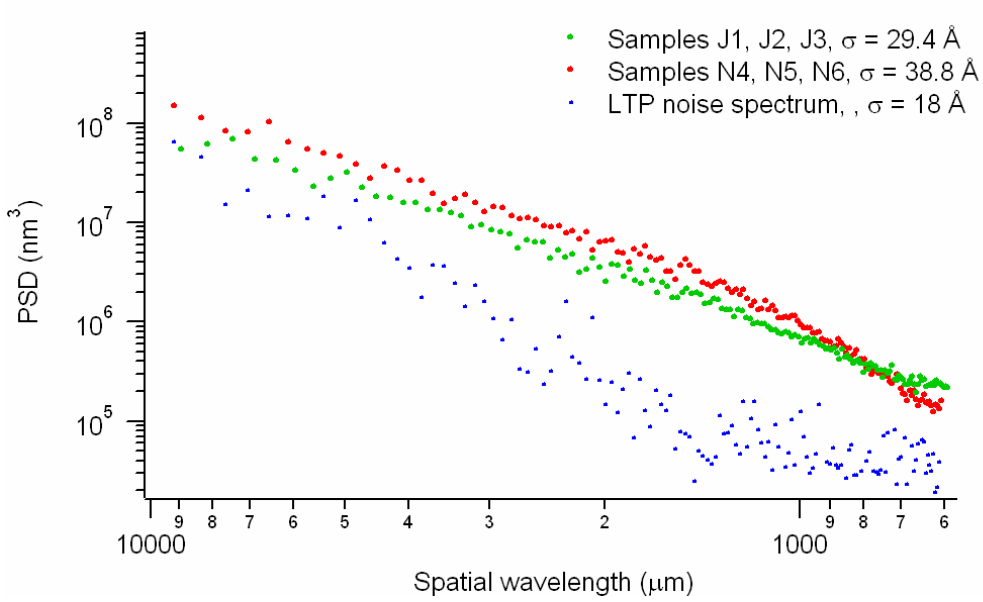

Fig. 2: the PSD of the samples under test as measured with the LTP profilometer. The instrumental noise spectrum has also been measured to check the measurement significance.

2.2 WYKO profiles

The roughness at average frequencies has been measured by means of the WYKO profilometer operated at INAF/OAB. The measurements have been performed at either 20x and 2.5x magnification, employing different instrument optical heads. Both sides of each sample were measured at 7 equally-spaced locations on each strip.

Due to an unavoidable misalignment of the optical head with respect to the sample surface, best-fit 1st degree polynomials was subtracted from 20x profiles, whereas at the 2.5x magnification, due to the more complicated structure of the interference fringes, best-fit 2nd order polynomials were subtracted from rough data.

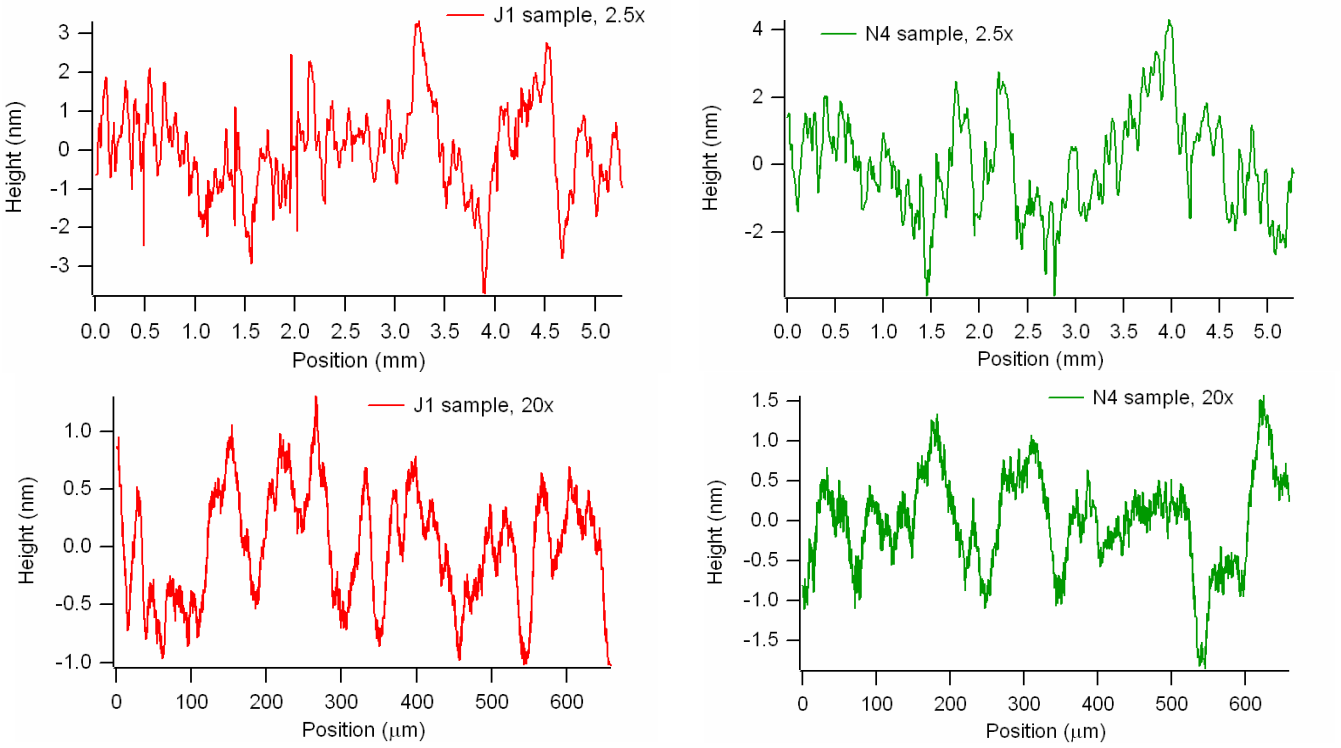

Fig. 3: some flattened WYKO profiles: (left) J1 sample and (right) N4 sample. (top) 2.5x magnification, (bottom) 20x magnification.

The resulting residuals are the sampled roughness in two different spectral regions: profiles recorded with the 2.5x magnification cover the spectral window 5.3 mm – 9 μm, whereas the 20x magnification is sensitive to the frequencies in the 660 μm – 1.3 μm range, even though the presence of some white noise at high frequencies limits the maximum observable frequency to 3 μm. On the other side, the 3 lowest frequencies in the 2.5 magnification have been damped out by the polynomial subtraction and have thereby been discarded from the dataset.

The PSD of each flattened profile and the resulting PSDs have been averaged over all 7 locations. The two sides of the samples have the same PSD within the measurement error, and the samples within each group (J and N) exhibit an uniform PSD as well. For this reason and for clarity's sake, we present only the average PSD for the two groups of samples in Fig. 4 and 5. We also plot the PSD derived from LTP measurements at lower frequencies.

The PSD obtained from WYKO at the two magnifications are in mutual agreement (with a slightly higher PSD for the 20x magnification between 100 and 10 μm) and they are also consistent with the LTP measurements: the overall PSDs nicely fit a power-law spectrum with a spectral index $n \sim 2$ (a value that falls exactly in the middle of allowed n values range for fractal surfaces, $1<n<3$).

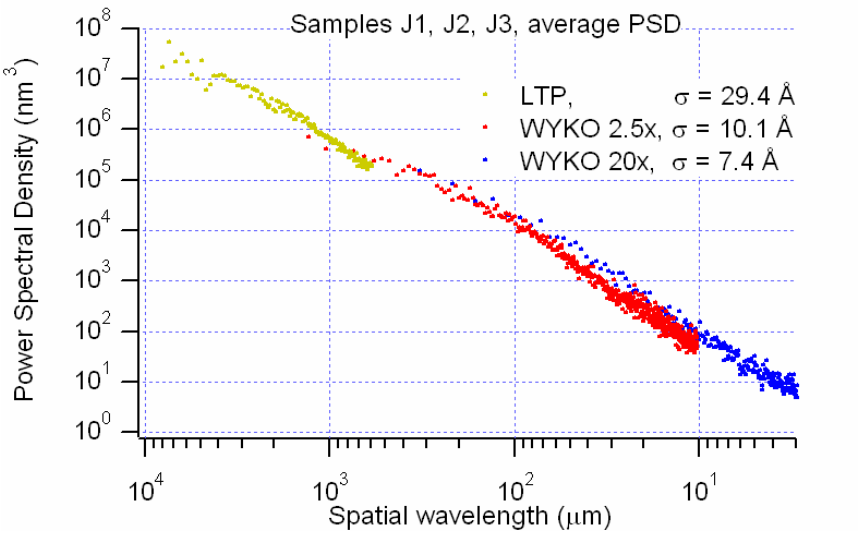

Fig. 4: the PSD of the sample J1 as measured with the LTP and WYKO (2.5 x and 20 x).

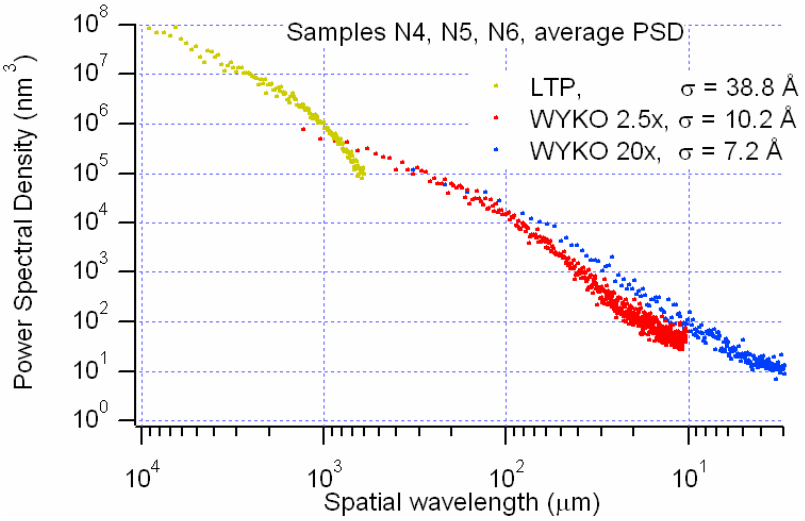

Fig. 5: the PSD of the sample N4 as measured with the LTP and WYKO (2.5 x and 20 x).

For the WYKO+LTP measurement, we can fit the PSDs obtained so far using the power laws. We retrieve the following parameters values:

$$P(f) = \frac{1.0 nm^3 \mu m^{-2}}{f^{-2}}$$

(J samples, WYKO+LTP)

$$P(f) = \frac{0.8 nm^3 \mu m^{-2.1}}{f^{-2.1}}.$$

(N samples, WYKO+LTP)

We also list in Tab. 2 the rms roughness for each sample side, computed from the integration of the PSDs, as measured with the WYKO profilometer.

Tab. 2: Silicon strips rms roughness values with the WYKO profilometer

Sample	***rms WYKO 2.5x (1500 - 10 μm)***	***rms WYKO 20x (330 - 3 μm)***
J1A	10.5 Å	7.4 Å
J1B	10.4 Å	7.8 Å
J2A	9.9 Å	6.9 Å
J2B	10.8 Å	7.1 Å
J3A	10.5 Å	7.4 Å
J3B	9.4 Å	7.3 Å
N4A	11.0 Å	6.4 Å
N4B	9.8 Å	7.7 Å
N5A	10.1 Å	6.8 Å
N5B	10.8 Å	7.9 Å
N6A	10.9 Å	6.7 Å
N6B	10.0 Å	7.2 Å

2.3 PROMAP – intermediate frequency roughness

We display in Fig. 6 two examples of PROMAP mapping of the samples under test, taken at *Media-Lario Techn.* at a 40x magnification. The sides of the images are 157×117 µm, and the sampling interval 0.25 µm,. For every sample, two points per sample side were mapped.

The silicon surface at these spatial scales exhibits an apparently smooth landscape, with wide undulations of 2-3 nm peak-to valley height. Some holes (5 nm deep, see Fig. 6, right) can be sparsely observed on the surface.

The PSD of the samples, that can be calculated down to 0.5 µm spatial wavelength, was computed along the X direction of the images for each available scan. As the PSD turned out to be quite similar within the two kind of samples ("J" and "N"), we averaged them to display a more representative PSD. We report, anyway, the rms roughness for each sample in Tab. 3, as derived from the integration of each PSD: the obtained values oscillate around $\sigma \sim 6$ Å. Also the PSD along y has been checked: however, the PSD computed in the y direction is known to systematically underestimate the highest frequencies in the PROMAP range. As a result, the rms computed from the PSD along y is also smaller (by 0.5 Å on average).

The computation results are shown in Fig. 7: the PSD of the "J" and "N" samples is consistent with WYKO for $\ell > 10$ µm, whereas WYKO clearly underestimates PROMAP data at higher frequencies.

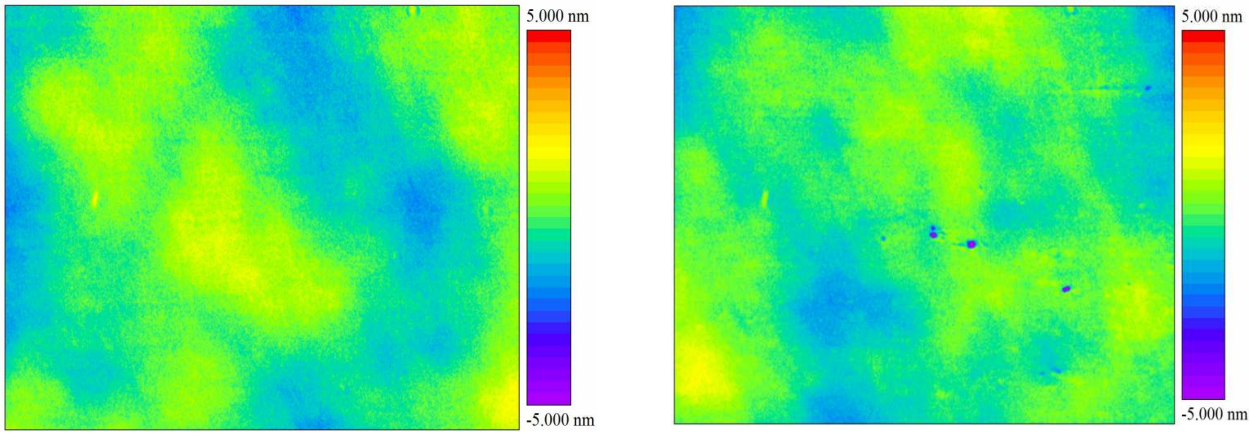

Fig. 6: two example PROMAP 40× maps of the Silicon surfaces (samples J1 – left and J2 - right). Map size: 157×117 μm. The surface relief seems to be dominated by smooth undulations. Rare holes (5 nm deep) are also present.

The two classes of samples exhibit, indeed, similar PSDs in the frequency window of PROMAP. Notice an important result: for both classes of samples, *a gradual slope change around 10 - 8 μm*, where the PSD spectral index passes from *2 ÷ 2.1* (see Sect. 2.2) to *~ 0.7*, a very low value. This slope change can have important consequences on the imaging degradation at high energies.

Tab. 3: Silicon strips rms roughness values with the PROMAP 40x optical profilometer ***(157 – 0.5 μm)***

Sample	***Rms roughness σ (from PSD)***
J1A	7.2 Å
J1B	5.7 Å
J2A	5.8 Å
J2B	5.8 Å
J3A	7.0 Å
J3B	5.2 Å
N4A	7.1 Å
N4B	5.2 Å
N5A	6.0 Å
N5B	7.7 Å
N6A	6.2 Å
N6B	7.1 Å

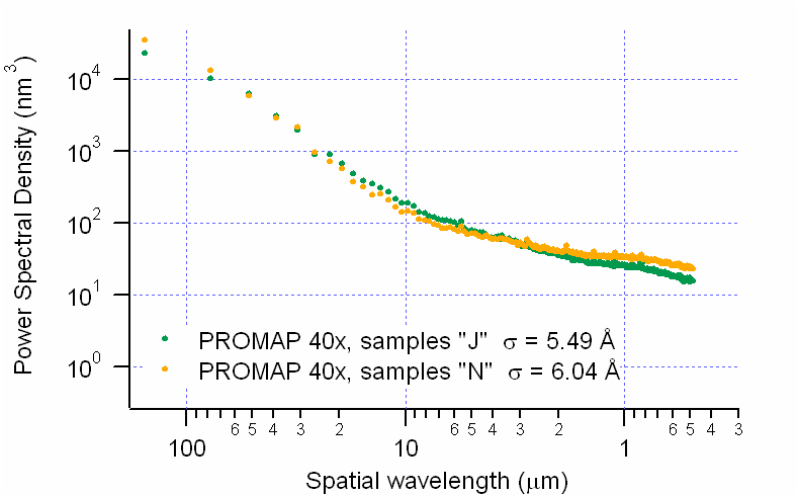

Fig. 7: the PSD of the samples, as measured with PROMAP. The two set of samples have a similar roughness.

2.4 AFM – high-frequency roughness

The sample roughness in the high-frequency regime has been measured with the stand-alone AFM Veeco – mod. Explorer, available at INAF/OAB in non-contact mode. The surface was probed with the non-contact technique, with 2 μm scans and a 5 nm lateral resolution: a typical surface map is shown in Fig. 8.

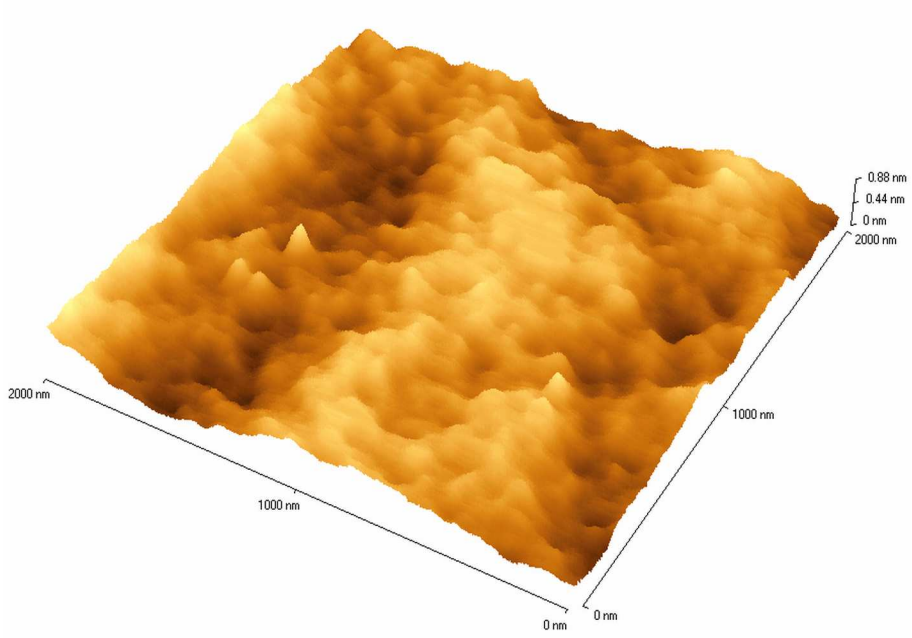

Fig. 8: A silicon surface landscape (the J3 sample, side A), as measured with AFM Explorer at INAF/OAB. The scan is 2 μm wide.

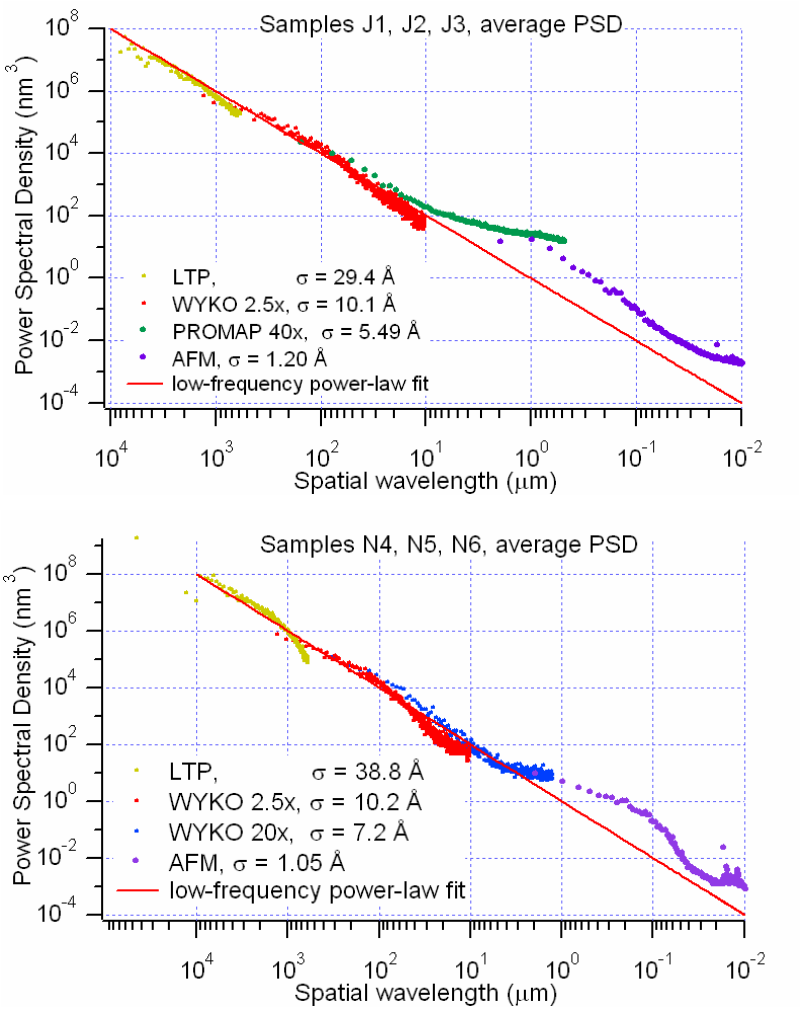

Fig. 9: The final PSD of the J samples (top) and N samples (bottom). The graph also includes the PSD derived from AFM and PROMAP measurements, and spans from 10^4 to 0.01 μm.

The AFM map exhibits a predominance of low frequency oscillations, even though high frequencies are also present. However, there is no evidence for point-like defects that had been observed with the Silicon sample previously analyzed [AD2], and which were responsible for the high roughness at high frequencies. The measured rms are reported in Tab. 4: in general, the results are good. The PSD analysis (see Fig. 9) shows that the AFM measurements are consistent with PROMAP/WYKO data, and that the actual PSD overestimates the one we could have inferred from the low-frequency power-law trend (see Sect. 2.2; also plotted, for comparison, in Fig. 9). Moreover, the "N" samples see to be slightly smoother at high frequencies. A result in common, indeed, is in that the PSD apparently exhibits a *doubly-broken power-law trend*, with an "ankle" at 20 μm spatial wavelength and a "knee" at 1 μm. This PSD will be discussed and compared with the one we measured in 2004 [AD2], in Sect. 4.1. Here we can at least state that the steeper slope of the PSD at high frequency helps limiting the degradation of the optics HEW, due to X-ray scattering, at high photon energies.

Tab. 4: Silicon strips rms roughness values with the AFM ***(2 – 0.01 μm)***

Sample	***Rms roughness σ (from PSD)***
J1A	N/A
J1B	1.21 Å
J2A	0.88 Å
J2B	0.67 Å
J3A	1.68 Å
J3B	1.41 Å
N4A	0.69 Å
N4B	1.30 Å
N5A	0.61 Å
N5B	1.10 Å
N6A	1.31 Å
N6B	0.93 Å

2.5. X-ray reflectivity measurements (XRR)

An independent evaluation of the surface roughness has been provided by means of X-ray reflectivity (XRR) measurement in grazing incidence, for variable incidence angles and a constant photon energy (8.05 keV, the Cu-Kα line), using the BEDE-D1 X-ray diffractometer operated at INAF/OAB. The X-ray beam at 8.05 keV is filtered from the bremsstrahlung spectrum emitted by a conventional X-ray tube with a Cu anode, using a *double* CCC Si crystal monochromators. A system of thin collimators in then used to select to produce a very thin (70 μm wide, 5 mm high) and parallel (~ 15 arcsec divergence) X-ray beam to probe the sample. Due to its very small size, the beam could be collected by the samples (10 cm long) even at very shallow (> 500 arcsec) incidence angles (see Fig. 10).

The samples alignment was carefully checked before data acquisition. The samples reflectivity was measured along with theta/2theta scans from 0 to 5000 arcsec, and collecting the reflected beam within a 800 μm wide slit at a 340 mm distance from the sample, corresponding to an half-aperture angle of $\Delta\theta_r$ = 240 arcsec. The measurement angular resolution equals the beam divergence (~ 15 arcsec).

The measured reflectivity has been fitted by means of standard numerical codes implementing modified Fresnel's formulae to account for X-ray scattering due to the surface roughness. Such a treatment enables the derivation of the rms roughness σ_R involved in reflectivity reduction, not the surface PSD.

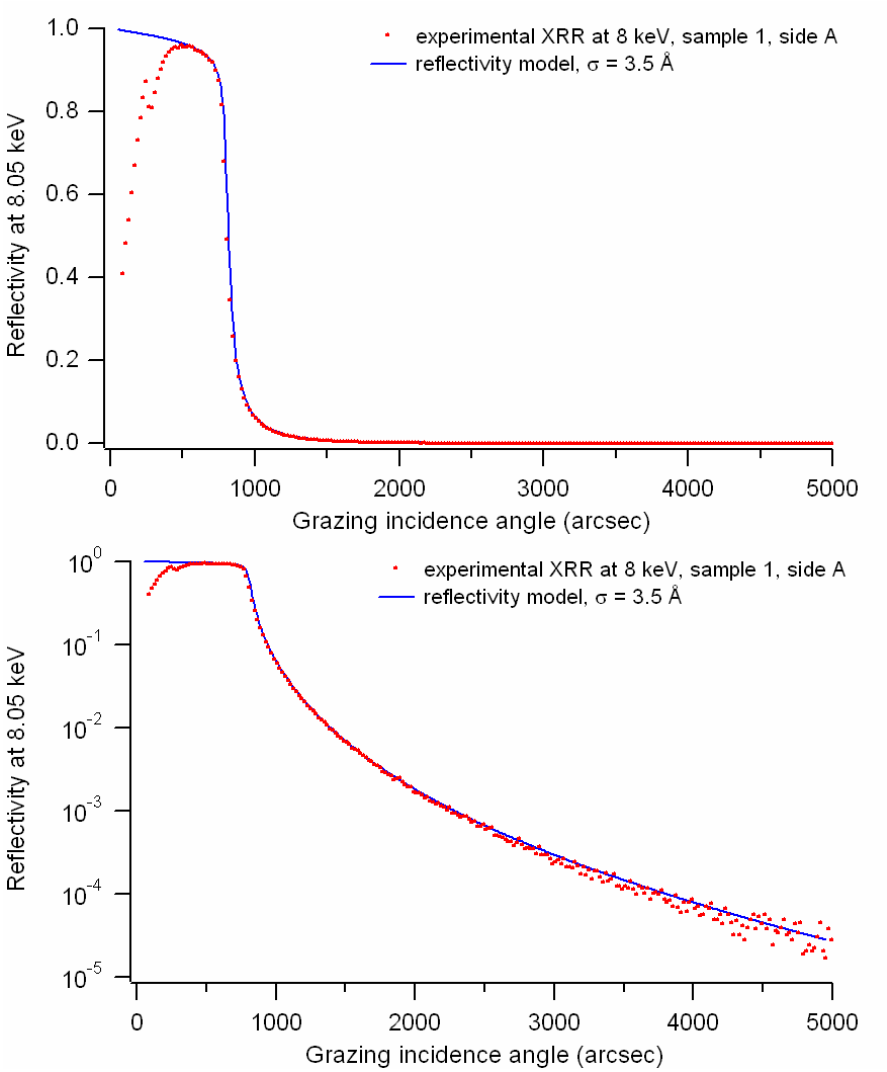

Fig. 10: the X-ray reflectivity at 8.05 keV of the sample J1, side A. The experimental reflectivity is well fitted by assuming a σ value of 3.5 Å. Linear plot (above) and log plot (bottom).

However, from the detector angular acceptance we can derive, from the usual grating formula

$$l_0 \approx \frac{\lambda}{\sin \vartheta_i \Delta \vartheta_r},$$

that the σ_R value should be referred to all wavelengths smaller than $l_0 \sim 10$ μm ($\lambda = 1.541$ Å and $\theta_i \cong 2500$ arcsec, i.e. the angle at which the reflectivity starts to sensitively change with the roughness in the present scans).

With some samples we could also detect the presence of a few nm-thick Si oxide, which results in weak interference fringes. The oxide thickness and the roughness values being inferred from fits are reported in Tab. 5.

Note that these rms values, although small, indicate that the actual samples PSDs *cannot be power-laws with n = 2 up to very high frequencies* (see Sect. 2.1 and 2.2). Were they fitting that model also at high frequencies, the rms values beyond $(10\ \mu m)^{-1}$ would be less than 1 Å. Therefore, the present XRR data analysis is consistent with a *slope change in the samples PSD at wavelengths shorter than a few micron. The PSD spectral index has to be smaller at high frequencies* in order to retrieve the required roughness level (Tab.5), as in fact we did observe with PROMAP and AFM (see Sect. 2.3 and 2.4). In fact, the integral of the PSD at frequencies larger than $(10\ \mu m)^{-1}$ returns 2.5 Å. This value is not far from the ones we found from the XRR fits, even if not completely consistent.

Tab. 5: rms roughness values and Si oxide layer thickness as inferred from XRR fits.

Sample	σ ***(l < 10 μm)***	Si_xO_y ***thickness***
J1A	3.5 Å	None
J1B	N/A	N/A
J2A	4.0 Å	2.0 nm
J2B	4.1 Å	2.2 nm
J3A	4.0 Å	2.2 nm
J3B	3.4 Å	0.2 nm
N4A	3.3 Å	0.5 nm
N4B	N/A	N/A
N5A	2.7 Å	2.2 nm
N5B	N/A	N/A
N6A	3.4 Å	2.0 nm
N6B	4.5 Å	1.0 nm

3. Multilayer-coated samples: characterization

In this section we present the measurements performed onto some multilayer-coated Silicon samples. The multilayers are graded Mo/Si multilayers, which consist of 113 bilayers couples. The multilayer has been conceived to return a smoothly-decreasing reflectivity for increasing photon energy at the incidence angle of 0.108 deg = 389 arcsec, and deposited by RF magnetron sputtering at INFN/LNL. Though widely used in EUV applications, Mo/Si multilayers are not optimal for astronomical X-ray optics coating, due to the absorption edge of Mo at 20 keV and the interdiffusion occurring at the interfaces Mo/Si which decreases the reflectivity effectiveness. Nevertheless, the deposition technique can be extended to couples of materials which suffer from these drawbacks to a much lesser extent, like W/Si and Pt/C.

Two samples have been deposited, with a nominal identical structure (named hereafter M140 and M143). Another sample with the same nominal structure (M150) has also been deposited later. The bilayer d-spacing decreases throughout the stack going from the multilayer surface to the substrate, along with 17 blocks of constant d-spacing. In this design (see Tab. 6), at a given grazing incidence angle, the outermost couples of layers reflect the softest X-rays, whereas the reflection of the hardest part of the X-ray spectrum takes place in the deepest part of the stack.

Tab. 6:nominal Mo/Si multilayer stack structure.

Block No. from surface	***No. of bilayers in the block***	***Si layer thickness (Å)***	***Mo layer thickness (Å)***
1	1	165	106
2	1	64	41
3	1	56	36
4	1	52	33
5	1	48	31
6	1	46	30
7	1	44	29
8	1	43	28
9	1	42	27
10	4	39	25
11	3	37	24
12	8	35	23
13	7	32	21
14	7	31	20
15	8	30	19
16	17	29	18
17	50	26	17

The number of bilayers in the blocks is not constant; rather, it increases as the d-spacing becomes smaller, because the number of bilayers necessary to return an effective reflectivity increases as the single-boundary reflectivity diminishes, i.e. for increasing photon energy. The thickness ratio of the two multilayer components $\Gamma = d_{Mo}/(d_{Mo}+d_{Si}) \approx 0.39$ is approximately constant in the stack.

The multilayer-coated part covers 2.5 cm in the central region (see Fig. 11) of the Silicon strips substrates (10 cm long).

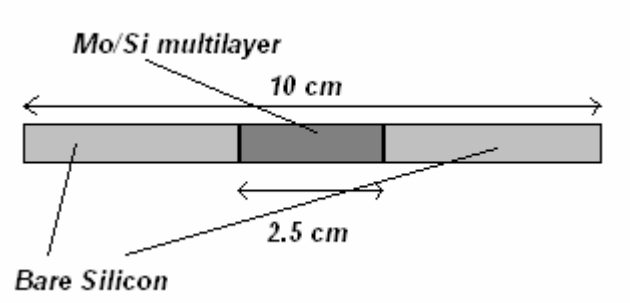

Fig. 11: Scheme showing the positioning of the multilayer coating.

3.1. X-ray reflectivity measurements (XRR) at 8.05 keV

The reflectivity of the deposited Mo/Si multilayer has been directly probed by means of a monochromatic (8.05 keV) X-ray beam using the BEDE-D1 diffractometer operated at INAF/OAB (Sect. 2.5). Since the diffractometer is not located in a dust-free environment, the sample was handled with a special sample holder enveloped in a thin Mylar film, which is almost transparent to X-rays at the energies in use. As the samples was handled and the envelope was closed only in a clean room, the sample was protected against dust contamination.

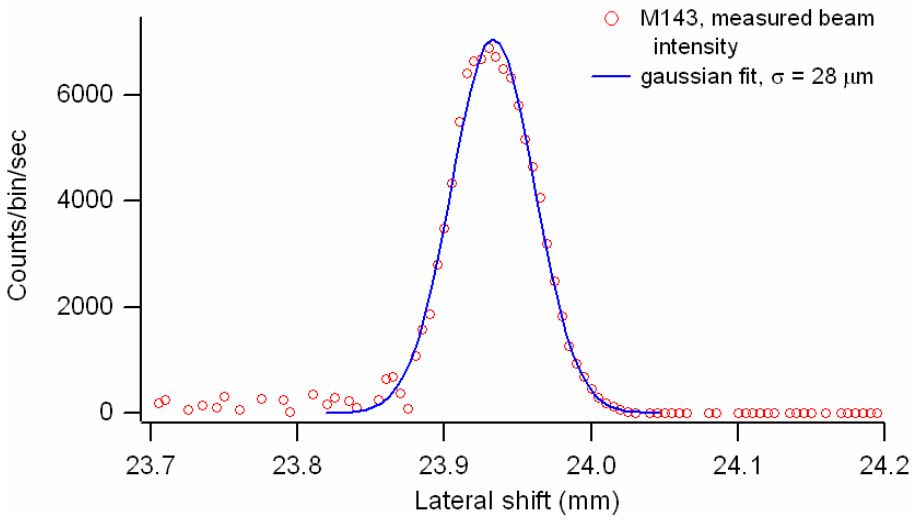

Fig. 12: the Gaussian profile of the beam used for the X-ray measurement at 8.05 keV .

Due to the small extent of the surface coated by the multilayer, the X-ray beam has to be very thin to be collected by the sample at very shallow grazing angles. Therefore, the incident beam has been limited by a properly-designed system of slits. After the beam shaping, its intensity has been recognized as a Gaussian profile with $\sigma = 28$ µm (see Fig. 12). As a consequence, 95% of the beam ($\pm 2\sigma$) is collected by the multilayer-coated surface at incidence angles larger than 4×28 µm/ 25 mm = 924 arcsec, not far from the critical angle for total external reflection.

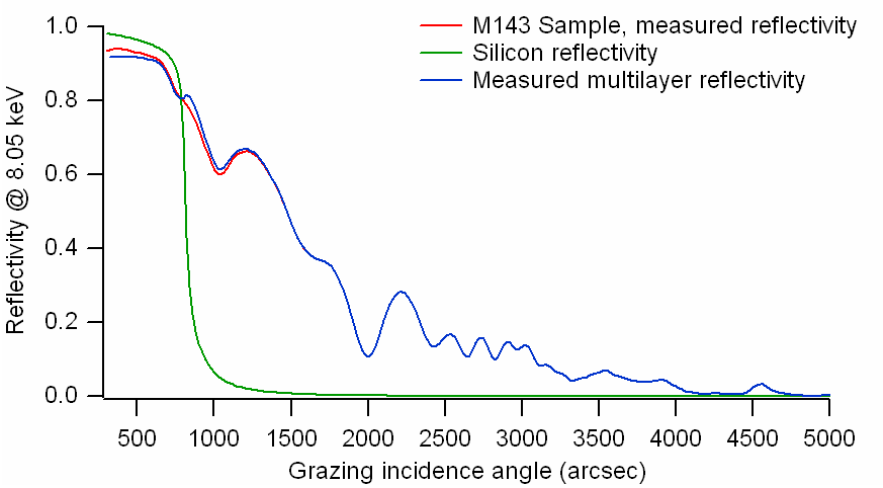

Fig. 13: the X-ray reflectivity at 8.05 keV of the sample M 143 (linear plot). Red line: the experimental reflectivity. Green line: calculated Silicon reflectivity. Blue line: the measured multilayer reflectivity, derived from the measured data and from the measured profile of the incident beam.

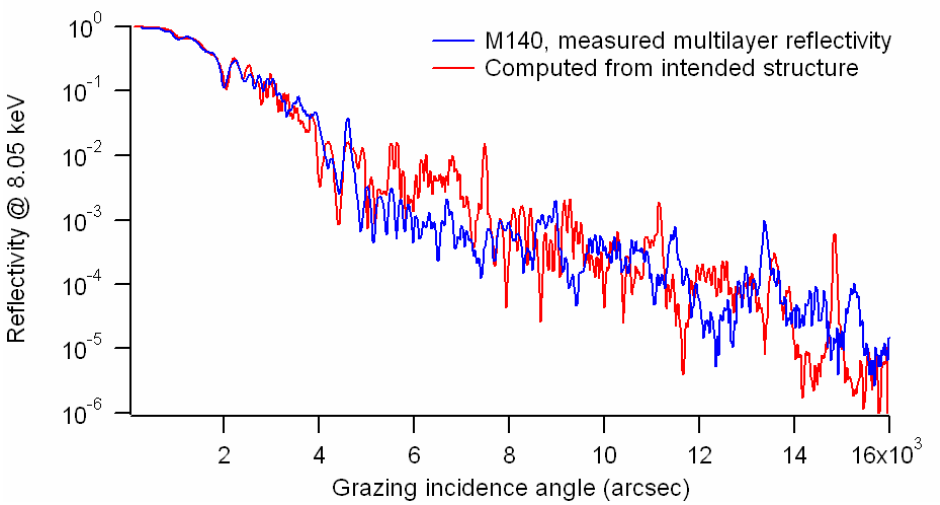

Fig. 14: sample M140: measured vs. computed multilayer reflectivity (logarithmic plot), assuming the recipe of Tab. 6 and 3 Å multilayer roughness rms. The departure of model (red) from data (blue) is due to some deviation of the actual structure from the intended design.

However, for small incidence angles, a non negligible amount of the X-ray beam falls on the uncoated Silicon. The experimental reflectivity will then be an average of coated and uncoated sample reflectivities, weighted over the respective fraction of surfaces illuminated by X-rays. The experimental reflectivity is plotted in Fig. 13 (red line). As we know the shape of the X-ray incident beam, by means of a straightforward calculation we can derive the reflectivity of the multilayer alone (Fig. 13, blue line). The multilayer reflectivity differs from the measured one only at angles smaller than 1400 arcsec.

The reflectivity scan of the multilayer M140 resembles very much that of the M143 sample, indicating that the structure of the two samples is similar. In Fig. 14 we plot the reflectivity of the multilayer M140, overplotted to the one calculated from the intended structure (Tab. 6), and assuming the natural densities of Mo (10.2 g/cm³) and Si (2.3 g/cm³) an effective roughness rms value σ = 3 Å (a value close to the one of the substrate). The agreement is good at very small angles, whereas at higher angles the two curves differ sensitively; this indicates some deviation of the actual structure from the intended one.

To derive a structure more representative of the multilayer stack, the reflectivity fit has to be refined, varying the thickness of layers until a satisfactory matching model-experiment has been reached. This has been semi-automatically done by means of the PPM program [RD3]. We still assume that there are no thickness drifts throughout the stack (i.e. the blocks are still rigorously periodic) but the layer thickness of the 17 blocks are let free to vary, starting from the nominal layer thickness (Tab. 6). The layer densities are still the natural ones, whereas multilayer roughness is also assumed as a variable, and an “intermixing layer” at each Mo/Si interface, of variable thickness also, has been inserted to account for layer interdiffusion.

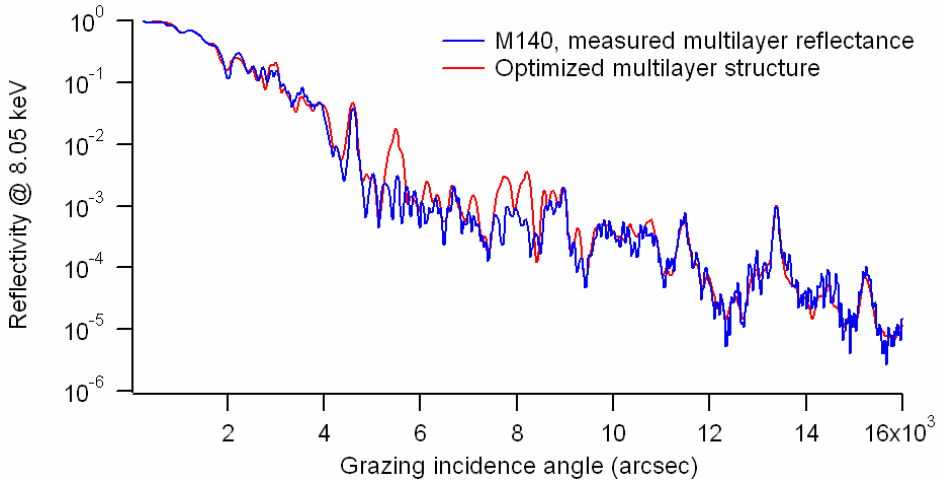

Fig. 15: sample M140; the refined reflectivity model (red) as derived from the application of the PPM program. The accord with experimental data (blue) has been improved with respect to Fig. 14.

After running PPM, the fit has been considerably improved: we show this in Fig. 15, in logarithmic scale (the improvement in linear scale is not so apparent): the result of the analysis is that the thickness of layers deviates from the nominal design (Tab. 6), by a variable amount. The

deviation is randomly-variable (non-systematic) within ± 5 Å. The remaining discrepancy model-experiment can be ascribed to an imperfect periodicity within the blocks. The model still fits the experimental data with a (constant) 3 Å roughness rms value, whereas the interdiffusion layer thickness is uncertain, but surely much less than 1 Å.

As a possible assessment of the deposition process, the multilayer does not seem to have increased the effective roughness of the surface. Moreover, the interdiffusion among layers is very low or even negligible. There could be, indeed, some problem with the stability of the deposition rate that could have caused the irregularities in the layers thickness values.

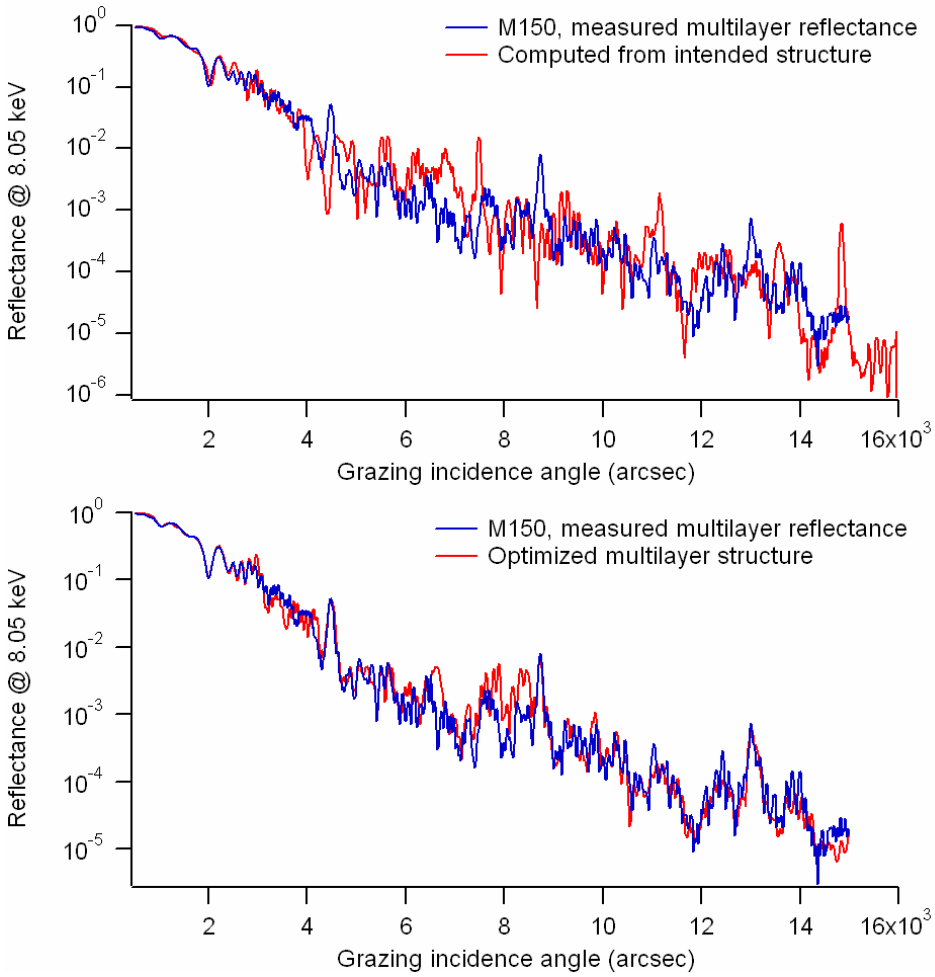

Fig. 16: sample M150.(top) initial comparison of the experimental reflectivity of the sample M150 with the initial recipe. (bottom) experimental vs. PPM findings.

We also plot in Fig. 16 the XRR measurement at 8.05 keV of the sample M150, deposited in a successive run. Similarly considerations as the samples M140 and M143 apply in this case. The analysis performed with PPM highlighted that the actual thickness trend deviates by ± 4/5 Å from the intended one. The deviations are quite random within the mentioned limits; similar oscillations should be encountered within the individual blocks and can be responsible for the residual discrepancies fit/experiment. The model still fits with a (constant) 3 Å roughness rms and < 1 Å interdiffusion.

3.2. X-ray reflectivity measurements (XRR) at 5 to 50 keV

The multilayer samples reflectivity has also been measured with the BEDE-D1 diffractometer in energy-dispersive setup at the incidence angle at which it was designed, 0.108 deg. The source was in this case a W-anode X-ray tube (biased at 50 kV) without monochromators. The very intense beam was shaped by means of a system of very thin slits: in this way we obtained a beam not too intense to avoid detector saturation and small enough (37 µm FWHM wide, 1 mm high) to be entirely collected by the detector entrance window (2 mm diam.). Also in this case the sample was protected against dust contamination by a Mylar envelope. The X-ray beam profile fits quite well a Gaussian profile with σ = 15.8 Å (Fig. 17), much narrower than that at 8.05 keV (Sect. 3.1).

The X-ray beam photon energy spans from 5 to 50 keV. The lower limit is dictated by X-ray absorption in the air. The detector was a Silicon energy-sensitive detector with a 0.149 keV sensitivity.

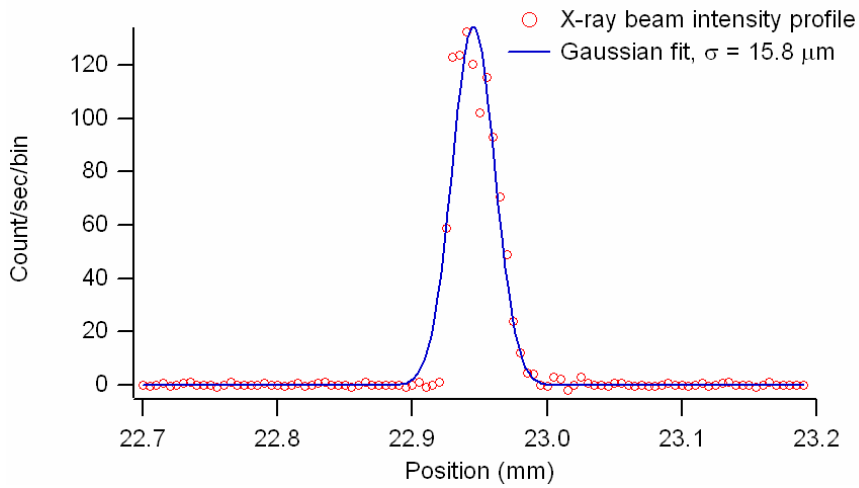

Fig. 17:the intensity of the polychromatic X-ray beam used for energy-dispersive measurements. The beam is narrower than that at 8.05 keV (see Fig. 12) in order to allow measurement at the very shallow angle of 0.108 deg.

Even if the X-ray beam is very thin, the small incidence angles causes the beam to be spread over a large portion of the sample, therefore some X-ray beam did fall on the uncoated Silicon. As we know the beam profile (Fig. 17) we deduce that the X-ray beam fall on the multilayer up to 1.5 σ.

This corresponds to 86% of the beam integral: the rest of the beam (14%) entirely falls on the Silicon, where it is reflected up to 16 keV (the critical energy of Silicon at 0.108 deg). With respect to the analysis of Sect. 3.1, disentangling the contribution of the multilayer is made easier by the fact that the fraction of beam falling onto the Silicon is constant at all energies.

The reflectivity measurement at the incidence angle of 389 arcsec are plotted in Fig. 18: the expected reflectivity from the multilayer structure (inferred from the analysis of reflectivity at 8.05 keV) is also overplotted, assuming that the effective roughness value is 10 Å. The agreement is imperfect, probably due to the imperfect modelization of the multilayer structure (it might correspond to the deviation of the model reflectivity in Fig. 15). The experimental reflectivity decreases smoothly for increasing photon energy.

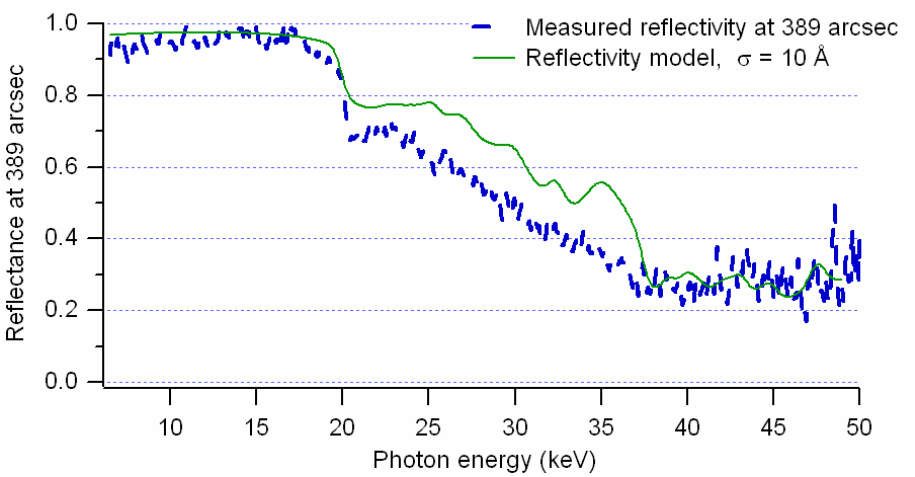

Fig. 18:the reflectivity of the multilayer sample M140 at 5 to 50 keV, at the incidence angle of 0.108 deg.

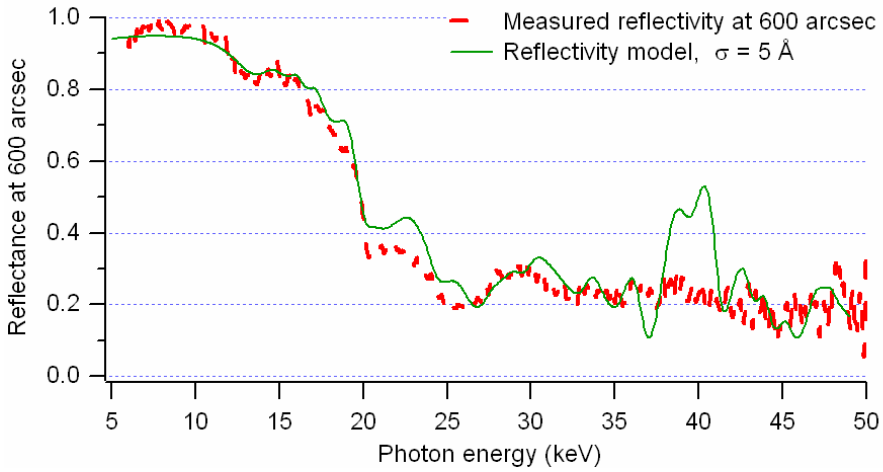

Fig. 19: the reflectivity of the multilayer sample M140 at 5 to 50 keV, at the incidence angle of 0.166 deg.

A check of the measurement correctness has been done by measuring the reflectance of the multilayer at 0.166 deg. At this grazing angle, all the X-ray beam falls on the multilayer without any contribution of Silicon. The measured reflectivity is plotted in Fig. 19. The reflectivity model inferred from the reflectance analysis at 8.05 keV applies well in this case, with a roughness rms effective value of 5 Å, at all energies but around 40 keV. The departure of the model from measured data might be due to some aperiodicity in the blocks, that was not considered in the model.

3.3. Surface roughness measurement: WYKO 2.5x and PROMAP 40x

The surface roughness of the multilayer samples has been measured with the WYKO (Sect. 2.2) and PROMAP (Sect. 2.3) optical profilometers. Due to local stresses in the multilayer stack or particle contaminations (Fig. 20), the PROMAP images in the 2.5x magnification were confused and could not be used. Therefore, WYKO was utilized at 2.5x magnification and PROMAP at 40x. The measurements for the samples were used to compute the PSD of the multilayer samples, which is being compared to that of the bare Silicon substrates in Fig. 21.

Excluding the most evident surface defects, the PSD computed for the sample M143 (Fig. 21, dots) exhibits some roughness growth with respect to the Silicon substrate (Fig. 21, red line). The comparison with corresponding data of Sect. 2.2 and 2.3 shows that the roughness increase is in fact very modest. WYKO data in the sample M140 did not exhibit any apparent roughness growth.

Measurements with AFM on multilayer samples have not been performed yet. They will be performed soon and added to the present dataset.

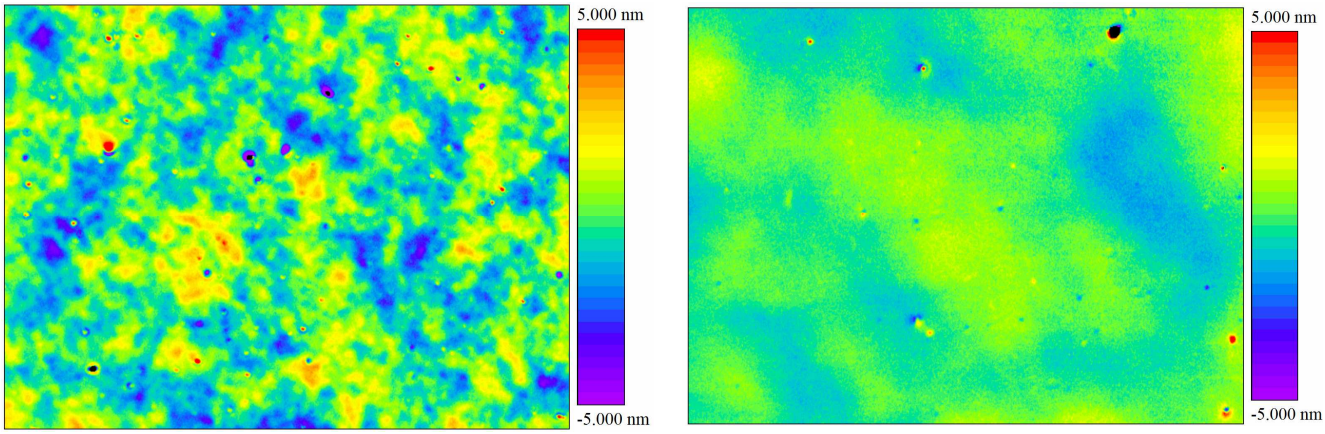

Fig. 20: some PROMAP images of the sample M140. The image in 2.5x magnification (2.5x) appears covered by surface defects. However (right),they do not appear at shorter spatial scales, in the 40x magnification. Since the defects which are been seen in the 2.5x map seem to be of no or little consequence on the reflectivity (Sect. 3.1), they are probably due to surface stress or particle contamination.

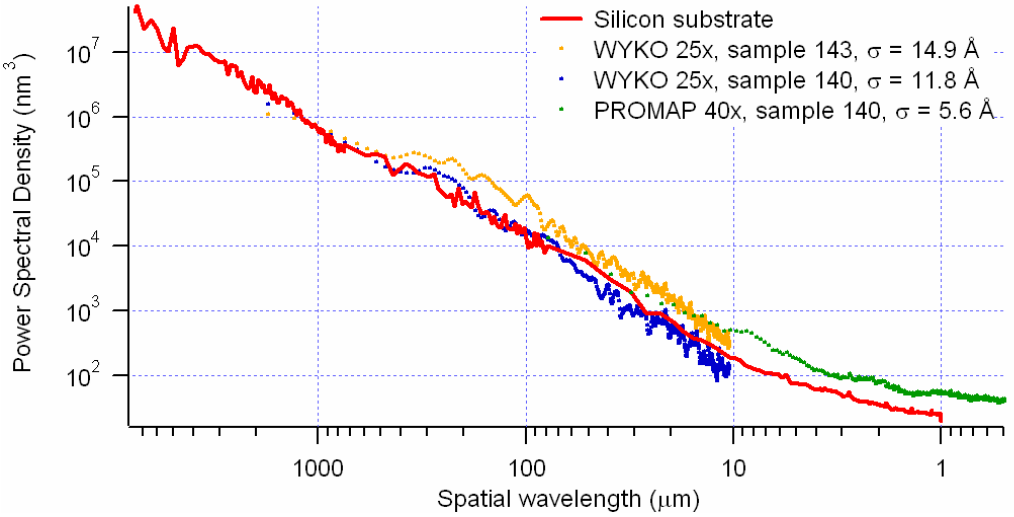

Fig. 21: comparison of PROMAP and WYKO roughness data at the multilayers surface with the PSD of the Silicon Substrates.

3.4. X-ray scattering measurements (XRS) at 8.05 keV

Also X-ray scattering experiments were performed on the multilayer samples, aimed at the indirect probing of the surface roughness. The scattering diagrams for the M140 and M143 samples turned out to be very similar, confirming the similar roughness properties of the two samples. A detector scan at 8.05 keV photon energy performed on the M143 sample at 2200 arcsec incidence angle is plotted in Fig. 22.

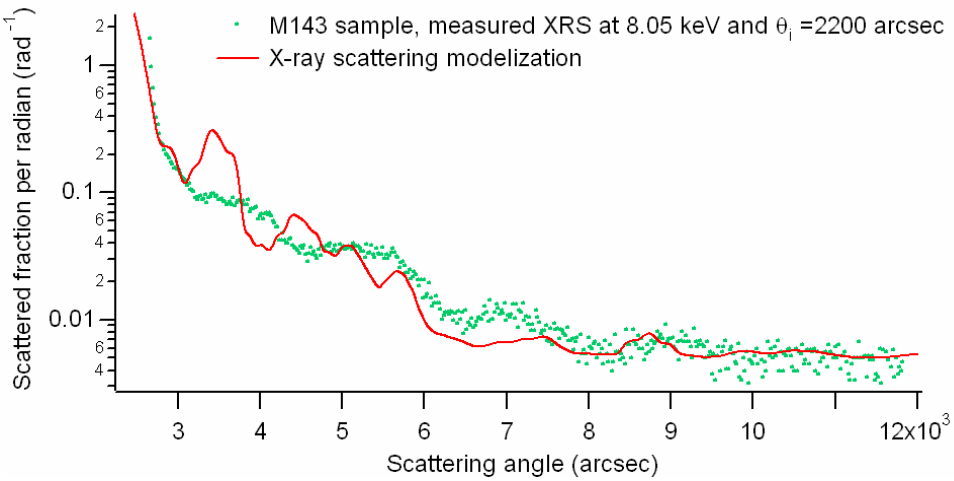

Fig. 22: XRS diagram measured on M143 multilayer sample, at 8.05 keV and at the incidence angle of 2200 arcsec (dots). Notice the oscillations in the scattering pattern due to the coherence of the rough profile throughout the stack and by the consequent interference of the scattered waves. The oscillations are roughly reproduced by the model (line).

Unlike the XRS pattern from simple substrates, the XRS from a multilayer coating may exhibit a complex structure due to the interference of X-rays scattered at each boundary Mo/Si and Si/Mo. The amplitude of the interference fringes - whose positions mimic to a large extent those of the reflectivity scan – is determined by the coherence degree among interfaces in the stack and on the evolution of the PSD throughout it, from the substrate to the multilayer surface. In Fig. 22 we overplot to the (normalized) experimental XRS data the prediction of a simple XRS modelization, assuming a constant and coherent PSD of the roughness throughout the stack. This assumption can be justified by the modest roughness growth observed in the Sect. 3.3 (even if AFM data are not available). The *substrates'* PSD was adopted to model the XRS diagram, and the multilayer recipe found from the XRR fit (Sect. 3.1) has been used to compute the phase and the intensity of the X-rays in the stack.

The resulting modelization is satisfactorily compliant to the experimental data, even if the amplitude and the position of maxima do not match perfectly. This can be caused, as previously stated, by aperiodicities in the blocks which the stack consists of (see Sect. 3.1), that were not considered in the XRS computation. Anyway, the magnitude of the calculated XRS is consistent with data, indicating a modest roughness growth through the multilayer coating.

4. Discussion of the PSD of *uncoated* Silicon samples. Expected HEW due to XRS for the XEUS optical module

4.1 PSD characterization comparison

In this section we briefly compare the PSD retrieved from the characterization of the ***uncoated*** Silicon samples analyzed in the present document with the results reported in [AD2], concerning the roughness characterization of the Silicon sample provided by ESA in 2004. The results are summarized in Fig. 23; the surface PSD of the samples (here we consider for simplicity only the average PSD of the "J" samples, see Sect. 2) analyzed in the present report is displayed in comparison with the model PSD of the Si strip of 2005. The main result is that the surface PSD are very similar at all frequencies *but for spatial wavelengths* smaller than 1 μm. At such high frequencies, the samples analyzed here are much smoother. In fact, they do not exhibit any longer the frequent, point-like surface defects that could be easily see in the AFM images of [AD2]. Also the X-ray data are consistent with a much smaller roughness value (Sect. 2.5) than that of 2005.

At *low frequencies* (ℓ > 20 μm) both PSDs are steep power-laws, with a spectral index close to 2. The quick decrease of the roughness power with increasing frequency is a merit factor since it enables a relevant reduction of the X-ray scattering at high energy that is responsible for the optical quality degradation with increasing photon energy [RD4].

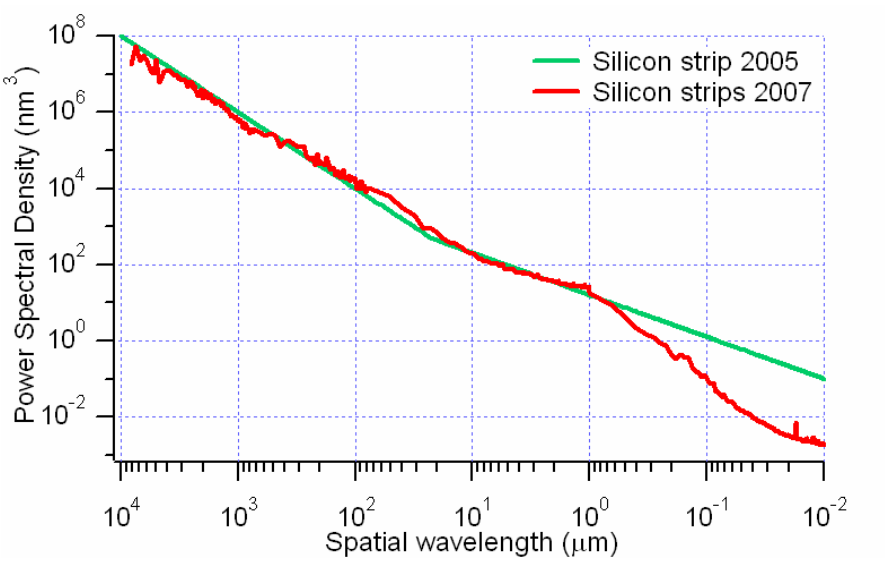

Fig. 23:the comparison of the roughness (modeled PSD) of the Silicon strip analyzed in 2005 [AD2] with that of the uncoated *samples investigated in the present study. There is an evident improvement at frequencies higher than (1 μm)*$^{-1}$.

At *intermediate* spatial frequencies (20 μm > ℓ > 1 μm) the two PSDs are still similar; the main feature is a relevant reduction of spectral index (< 0.8), that implies a much important

contribution of the PSD to higher frequencies than expected by extrapolating the low-frequency power-law model.

At *high frequencies* (ℓ > 1 μm) the two PSD apparently diverge from each other: the PSD of 2005 keeps its smooth decrease whereas that of 2007 exhibits a cut-off. Therefore, the PSD of 2007 deviates from a power-law by a "bump" that would significantly increase the high-frequency content with respect to the power-law model. It represents, indeed, a significant improvement with respect to the PSD of 2005.

4.2 From the PSD to the expected HEW

The PSD characterization over a wide spectral range also enables us to calculate the HEW of the XEUS optical module, as expected from the surface finishing of the *uncoated* samples. Assuming a 5 arcsec figure error contribution to HEW (energy-independent), the XRS contribution to the HEW – as a function of the photon energy - can be calculated for each mirror [RD4] and added in quadrature to return the total HEW of the mirror. Then the overall HEW of the XEUS optical module can be obtained averaging the obtained HEW trends over the mirrors effective area (we hereby refer to the XEUS optical baseline with a 35 m focal length).

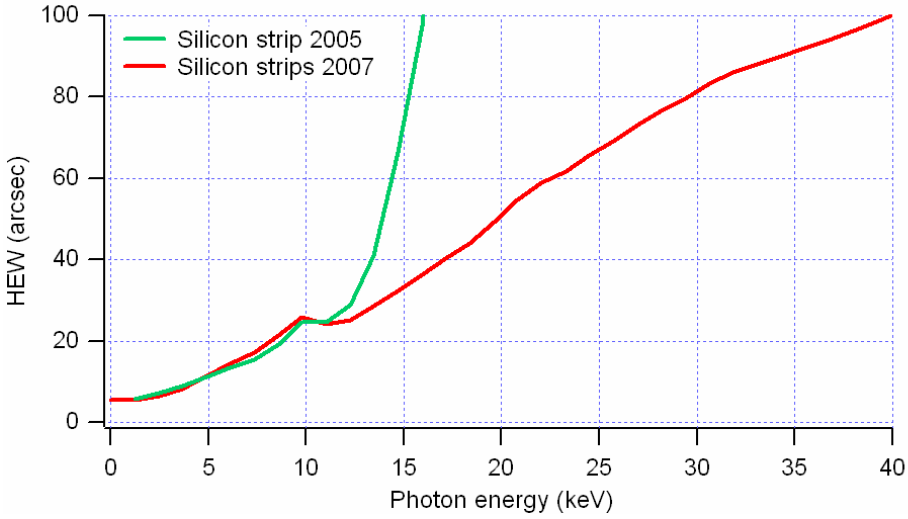

Fig. 24: calculated HEW trends from the PSD plotted in Fig. 23 for the XEUS optical module, assuming a 5 arcsec figure error HEW.

The calculation results are plotted in Fig. 24. Even if there is still an increase of the HEW with photon energy, this is much smaller for the PSD measured in the present campaign than for the case of 2005. The improvement (apparent beyond 13 keV) is essentially due to the better smoothness of the surface at high frequencies, and it makes apparent the importance of a sharp cut-off of high frequencies in manufacturing high-quality X-ray optics.

4.3 Conclusions

The performed analysis can be summarized as follows:

1. The Silicon samples surfaces and profiles were extensively characterized over spatial scales from 10^4 µm to 10 nm (Sect. 2). The analysis in terms of PSD lead to mutually-compliant results from instruments with different sensitivity bands (AFM, WYKO, PROMAP). In addition, the results have been checked by means of independent XRR analyses (Sect. 2.5).
2. The PSD of samples is quite homogeneous. The PSD in general fits a doubly-broken power law, with slope changes around 20 and 1 µm. When compared with the corresponding sample of 2005, one can observe in the present samples a clear improvement at high frequencies (Sect. 4.1). This has, in turn, important consequences on the expected degradation of imaging quality for increasing photon energies (Sect. 4.2), caused by X-ray scattering, that becomes the dominant term of the HEW in hard (> 10 keV) X-rays.
3. Graded Mo/Si multilayers could be successfully deposited onto Silicon substrates (see Sect. 3). The X-ray reflectivity of coatings at either fixed or variable photon energy is satisfactory (Sect. 3.1 and 3.2), with a very relevant enhancement of the X-ray reflectance of the samples up to 50 keV. X-ray scattering measurements (Sect. 3.4) showed that the roughness growth throughout the stack should be very modest. There might be, indeed, some problems related to the deposition rate stability of the facility employed to deposit the multilayer onto the samples, resulting into irregularities of the layer thickness. Future developments of the activities should be aimed, moreover, at mitigating interfacial stress (Sect. 3.3) in the multilayer.